



ELSEVIER

Available online at [www.sciencedirect.com](http://www.sciencedirect.com)

SCIENCE @ DIRECT®

Journal of Luminescence 107 (2004) 62–74

JOURNAL OF  
LUMINESCENCE

[www.elsevier.com/locate/jlumin](http://www.elsevier.com/locate/jlumin)

# Multi-Gigahertz radar range processing of baseband and RF carrier modulated signals in Tm:YAG

K.D. Merkel\*, R. Krishna Mohan, Z. Cole, T. Chang, A. Olson, W.R. Babbitt

*Spectrum Lab, Montana State University, P.O. Box 173510, Bozeman, MT 59717, USA*

## Abstract

An optical device is described and demonstrated that uses a spatial-spectral holographic material to perform coherent signal processing operations on analog, high-bandwidth optical signals with large time-bandwidth-products. Signal processing is performed as the material records the coherent spectral interference (or cross-power spectrum) of modulated optical signals as a spatial-spectral population grating between electronic transition states. Multiple exposures of processing pulse sequences are integrated with increasing grating strength. The device, coined as the Spatial-Spectral Coherent Holographic Integrating Processor (or S<sup>2</sup>-CHIP), is described as currently envisioned for a broadband, mid-to-high pulse repetition frequency range-Doppler radar signal processing system. Experiments were performed in Tm:YAG (0.1 at% at 5 K) to demonstrate time delay variation, integration dynamics, and effects of coding as applied to a radar range processor. These demonstrations used baseband modulation with a 1 gigabit per second (GPBS) bit rate and code length of 512 bits (512 ns), where delays up to 1.0 μs were resolved with greater than a 40 dB peak to RMS sidelobe ratio after 800 processing shots. Multi-GHz processing was demonstrated using a bit rate of 2.5 GBPS (baseband modulation) and code length of 2048 bits (819.2 ns). Processing of double-sideband modulated signals on a radio frequency (RF) carrier was demonstrated, where 512 bit, 1.0 GBPS codes were modulated on a 1.75 GHz carrier and then modulated on the optical carrier.

© 2004 Elsevier B.V. All rights reserved.

*Keywords:* Analog optical signal processing; Radar signal processing; Range correlation; Doppler processing; Optical coherent transients; Spatial-spectral holography

## 1. Introduction

Optical devices using rare earth doped crystal-line spectral hole burning materials have recently shown promise for wideband bandwidth applications, with coherence times of tens of microseconds, integration times of several milliseconds, and large material dynamic range, in areas of RF

signal processing [1], RF spectrum analysis [2], atmospheric sensing [3] and true time delay or arbitrary waveform generation [4,5] among others. For high bandwidth analog RF signal processing, the optical approach presents a distinct advantage over digital techniques, since no high bandwidth analog to digital converter (ADC) is needed or used. The device being developed by our group, coined as a Spatial-Spectral Coherent Holographic Integrating Processor (S<sup>2</sup>-CHIP), aims to achieve analog signal processing for applications arenas such as ultra-wideband range-Doppler radar processing with noisy waveforms and frequency

\*Corresponding author. Tel.: +1-406-994-7241; fax: +1-406-994-7980.

E-mail address: [merkel@spectrum.montana.edu](mailto:merkel@spectrum.montana.edu) (K.D. Merkel).

agile radar. The approach could be extended to solve other signal processing problems in other applications, such as for radio astronomy and lidar. Our discussion in this paper concentrates on radar range signal processing.

One practical aspect of the device comes from being able to process high bandwidth signals (multi-GHz) that are modulated on radio frequency (RF) carriers, as well as baseband RF signals. In either case, the signals are modulated onto an optical carrier and then irradiate the processing crystal. The crystal performs signal processing by holographic recording of the power spectrum of the input light sequence as a spatial-spectral ( $S^2$ ) grating. The optical transition's persistence allows for recording the integration of multiple exposures, or shots. The resultant  $S^2$  grating is read out using a linear frequency chirped optical pulse, creating a low bandwidth (tens of MHz) oscillation of the optical intensity. This approach leverages both the wide material bandwidth for processing, and mature, inexpensive photodetector and digitizer technologies at low-bandwidths for readout. This feature presents a distinct advantage over previous designs, with no requirement for high bandwidth optical-to-electronic converters or ADC.

Following is an overview of the general device design and operation as it is currently envisioned and a description of recent experimental results. Performed in Tm:YAG at 5 K, these results reflect proof of concept efforts for radar range processing of binary phase shift keying (BPSK) signals, both using baseband modulation at 1.0 and 2.5 GBPS, and the first demonstration of optical processing of signals first modulated on an RF carrier, using a 1.0 GBPS bit rate modulated on 1.75 GHz. In all results presented here, the readout window bandwidth was limited to 40 MHz, which will be extended in future efforts.

## 2. $S^2$ -CHIP operation and considerations

### 2.1. $S^2$ -CHIP description and design for radar

Fig. 1 shows a simple schematic of the  $S^2$ -CHIP operating as a radar processor. In a monostatic

radar system, a pulse generator creates an optimally encoded baseband waveform that is modulated onto an RF carrier  $\nu_{\text{RF}}$  and then transmitted. The antenna later receives the scattered signal return from the target that is delayed, attenuated, Doppler shifted, and buried in a noisy background including broadband noise and narrowband jammers. Analog correlation of the received signal with a properly timed reference signal (delayed by  $\tau_{\text{off}}$ ) determines the delay  $\tau$  between them, yielding the target's range  $R = c(\tau + \tau_{\text{off}})/2$ , where  $c$  is the speed of the radiation. In a repetitively pulsed radar system with a pulse repetition interval  $T_{\text{R}}$  and corresponding pulse repetition frequency  $\text{PRF} = 1/T_{\text{R}}$ , the integration of the processed information of multiple coherent returns increases the signal-to-noise ratio (SNR) of the result and reveals effects of Doppler shifts  $\nu_{\text{D}} \approx (-2V/c)\nu_{\text{RF}}$  on the target return(s) from the original RF carrier, where  $V$  is the speed of the target [6,7]. Multiple PRFs can be used to eliminate ambiguities.

For optical processing of radar signals, transmit and return RF signals are each modulated on a stable (coherent) optical carrier. The modulation from the RF domain to the optical domain is achieved by an electro-optic phase modulator (EOPM), which changes the optical carrier phase in proportion to the applied RF voltage. One modulator is used for the reference waveform, a replica of the transmit waveform with appropriate timing and predistortion for optimal matched filtering. A second modulator is used to modulate the received signal from the radar returns. The modulated optical carrier is tuned to the transition resonance of the  $S^2$  crystal and the optical beam is focused to a diffraction-limited volume (i.e., a spatial channel) in the crystal for processing. The material experiences and records a spatial-spectral interference of the optical waveforms and stores the result as a frequency dependent population grating. The population state persistence allows for that result to persist, and for other operations to take place. Integration of multiple results increases the SNR of the processed results, and can be used to resolve Doppler shifts on target returns. Full range-Doppler processing can be achieved using parallel spatial channels with

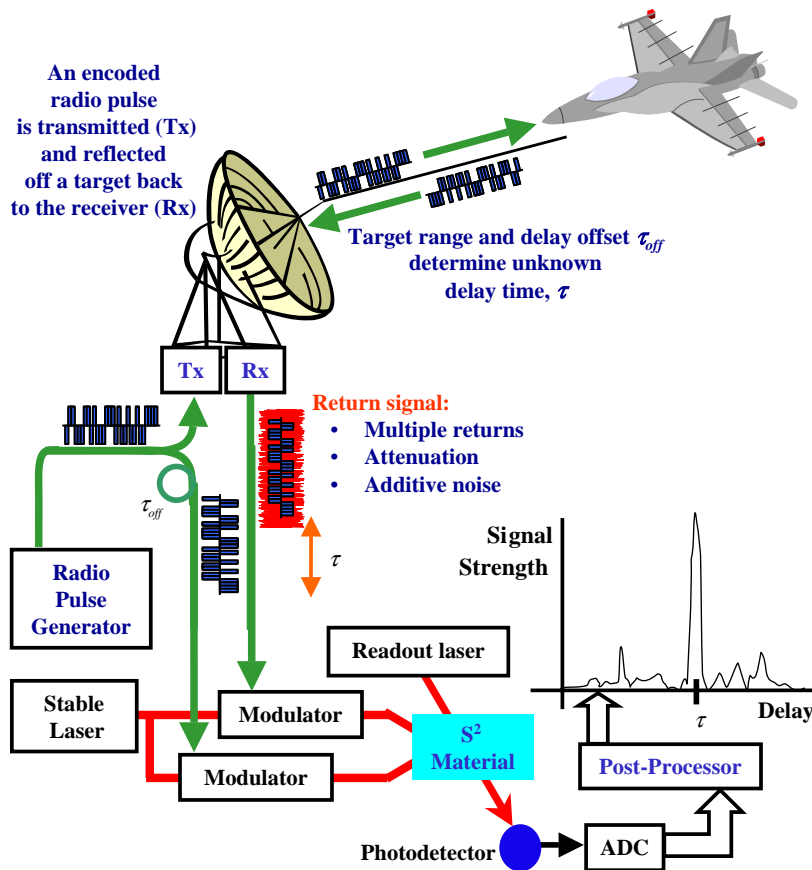


Fig. 1. Operation of  $S^2$ -CHIP range processor in a single antenna element radar system.

frequency shifted reference pulses corresponding to Doppler frequency bins.

During the time that the integrated grating persists, the result can be read out with an appropriate spectral scan (i.e., linear frequency chirp) of the absorption band. This readout approach produces a low bandwidth oscillatory variation on the optical intensity that represents the grating strength and structure. Such low bandwidth readout signals can be measured with large dynamic range using a photodetector and digitized with high precision. A power spectral density (PSD) algorithm yields the spectral content, and which scaled by the reciprocal of the chirp rate yields the processed delays. Since the return signal can be from multiple targets, the post-processed output is a range profile showing the delays and strengths of all the targets over the

range of interest. The full range-Doppler ambiguity function is compiled by combining the range profiles of each spatial processing filter.

## 2.2. $S^2$ materials and radar system specifications

The intrinsic spectroscopic properties of the  $S^2$  material will govern the processing, integration, and readout stages and largely define the radar processing system performance. Material transition parameters of specific interest include the resonance wavelength, the inhomogeneous line width, coherence time  $T_2$ , the population lifetime  $T_1$ , and doping density. Currently, the  $S^2$ -CHIP demonstrator utilizes Tm:YAG on the  $^3H_4$ - $^3H_6$  transition at 793.380 nm, but could also be performed near 1550 nm in Erbium doped crystals [1].

### 2.2.1. Processing bandwidth

The system instantaneous processing bandwidth  $B_P$  and the frequency band coverage will be limited by the  $S^2$  material bandwidth, which is determined by the inhomogeneous broadening of dopant ion resonances in the host lattice. In Tm:YAG (0.1 at%), the full-width at half-maximum value of the absorption line is  $\sim 30$  GHz, and can be varied by compositional tuning in the growth process. From a system's perspective,  $B_P$  is limited by hardware implementation, including the driving electronics and electro-optic modulators. The delay resolution of the radar is  $\sim 1/B_P$  depending on the SNR of the received signals [6,7].  $S^2$  materials therefore offer the potential for very high range resolution processing.

Large frequency coverage, or a large aggregate bandwidth, can be utilized by processing many band-limited RF signals modulated on various intermediate frequency (IF) carriers, in parallel, across the material bandwidth. The full use of the material bandwidth is also desirable for being able to sense and process signals of a frequency hopping radar system.

### 2.2.2. Coherence time

For any single shot exposure of waveforms to the material, the material coherence time  $T_2$  (also called the homogeneous broadening lifetime) directly affects the effective coherent processing time. The value of  $T_2$  is a complex function of the temperature, material bandwidth, excitation bandwidth, dopant density, and incident optical power, among other factors. In Tm:YAG (0.1 at%) under typical operation conditions,  $T_2 \sim 10$   $\mu$ s.

### 2.2.3. Population lifetime

The population lifetime  $T_1$ , or memory time of the material, directly affects both the integration time and the readout time. In Tm:YAG (0.1 at%),  $T_1 \sim 10$  ms. Within this time window, both processing by integration and readout are completed. The number of integrated shots by the material is the product of the integration time and PRF. For example, given PRF = 50 kHz and  $T_1 = 10$  ms, up to 500 shots could be integrated. The actual number of desired integrated shots for coherent radar is limited by the target coherence time. The

Doppler shift resolution is  $\sim 1/T_1$  as obtained from processing and integration and the SNR [6,7].

### 2.2.4. Doping density

The dynamic range of the material for recording spectral gratings depends on the available absorption ions in the material, and their probability of interaction with the incident processing photons. The ions per unit frequency per unit volume,  $\Upsilon$ , is a material parameter that depends on the doping density and host. As an example, for Tm:YAG (0.1 at%) with a 30 GHz Gaussian lineshape,  $\Upsilon \sim 4 \times 10^{14}$  ions/(Hz  $m^3$ ) over the central 20 GHz bandwidth. Using a typical processing volume of  $8 \times 10^{-11}$   $m^3$ , (a  $\sim 100$   $\mu$ m diameter spot ( $1/e^2$  width) over 10 mm of crystal length) there are  $3.2 \times 10^9$  ions/MHz. Variation in the interaction volume and/or doping density can be considered for higher spectral selectivity specifications.

## 2.3. $S^2$ -CHIP operation

### 2.3.1. Processing of RF radar waveforms modulated on optical carriers

Consider a radar system transmitting a series of broadband BPSK modulated waveforms and then receiving a superposition of attenuated, range delayed and Doppler shifted returns with noise and possible jammer tones present.

In general, coded waveforms are used to provide processing gain. The larger the ratio of the peak strength of the auto-correlation function to the temporal sidelobes, the greater the processing gain. While the pulse modulation can be in amplitude, frequency (e.g., frequency hopped or linear-chirped), or phase (biphase, polyphase, etc.), high bit rate BPSK modulation is readily achievable using modern electronics. The BPSK modulation waveform characteristics are determined by the modulating code used and the shape of the pulse waveform. Codes are specified by their length of  $N$  bits, modulated at the bit rate  $R_B$ , with waveform duration  $\tau_p = (N/R_B) < T_R$ . Any binary codes can be used, including pseudo-random noise (PRN) sequences. For a typical  $N$ -bit BPSK PRN sequence, the autocorrelation peak has amplitude

$N$ , and the RMS sidelobe level has amplitude  $\sim \sqrt{N}$ .

The modulating waveform of the  $j$ th shot in the transmit series is first considered. The baseband signal is a voltage waveform

$$m_j(t') = \sum_{n=0}^{N-1} a_n^j c\left(t' - \frac{n}{R_B}\right), \quad (1)$$

where  $a_n^j$  is binary code set of the  $j$ th shot (taking a value of either  $-1$  or  $+1$ ),  $n$  is the bit index,  $c(t')$  is the bit voltage waveform, and  $t'$  is the time relative to the start of the shot. This baseband signal is modulated on a RF carrier for transmission from the antenna as

$$s_j(t') = m_j(t') \cos(\omega_{RF} t'), \quad (2)$$

where  $\omega_{RF} = 2\pi\nu_{RF}$ . For the following analysis, a generalized voltage function is defined as the reference “transmit” waveform of the  $j$ th shot as

$$V_j^T(t') = p_j(t' - jT_R), \quad (3)$$

where  $p_j(t')$  represents either  $s_j(t')$  or  $m_j(t')$ .

After being transmitted, a target can reflect the signals back to the radar receiver antenna. While multiple target returns are possible, each with their own attenuation and delay, here a single target return delayed by a time  $\tau$  is assumed. The goal of the processor is to determine this unknown delay, in order to calculate the target's range. To further simplify the analysis, the target return is assumed to have no narrowband jammers, Doppler shifts or waveform dispersion. In this case, the received “return” signal for the series is

$$V_j^R(t') = G[ap_j(t' - \tau - jT_R) + n(t')] \quad (4)$$

which represents the signal on the RF carrier or at baseband, where  $a$  is the attenuation of the return signal,  $n(t')$  is broadband additive noise on the return signal, and  $G$  is a gain factor.

For each shot  $j$ , the transmit and return signals are modulated onto an optical carrier which irradiates a spatial volume of the  $S^2$  material. An EOPM is used to modulate the electrical signal  $V(t)$  onto an optical carrier  $\omega_L$  as  $E_0 \exp(i[\omega_L t + \beta V(t)])$ , where  $\beta$  is a linear electro-optic conversion coefficient. In practice, two EOPMs would be used, one each for the transmit and return signals,

to create two optical beams that are overlapped at a small angle.

For simplicity, the case of single EOPM is analyzed below and used in the experimental work. When both the transmit and return signals are modulated by a single EOPM, then the field of that carrier can be written as

$$E_j(t') = E_0 \left( e^{i(\omega_L t' - \beta V_j^T(t'))} + e^{i(\omega_L t' - \beta V_j^R(t'))} \right) \quad (5)$$

where  $E_0$  is a slowly varying amplitude on the optical carrier. If phase modulation remains in the linear regime (if  $\beta|p_j(t)|$ ,  $\beta G a|p_j(t)|$ , and  $\beta G|n(t)| \ll 1$ ), then the optical signal for each shot of the radar can be approximated as

$$E_j(t') \approx E_0 e^{i\omega_L t'} [(1 - i\beta p_j(t' - jT_R)) + (1 - iG\beta(ap_j(t' - \tau - jT_R) + n(t')))]. \quad (6)$$

To understand the processing stage, consider a single transmit and return coded waveform pair, the  $j$ th pair in the series, as a single shot of optical waveforms that interact with the absorbing  $S^2$ -material. The optical power spectrum of the  $j$ th shot is

$$P_j(\Delta) \propto |E(\Delta)|^2 \approx \beta^2 E_0^2 [(1 + G^2 a^2 + 2Ga \cos(\Delta\tau)) \times |\tilde{p}_j(\Delta)|^2 + G^2 |\tilde{n}_j(\Delta)|^2 + G(\tilde{n}_j^*(\Delta)\tilde{p}_j(\Delta)e^{i\Delta(jT_R)} + \text{c.c.})] \quad (7)$$

where  $\tilde{p}_j(\Delta)$  and  $\tilde{n}_j(\Delta)$  are the Fourier transforms of the coded waveform and noise, respectively, and  $\Delta = \omega - \omega_L$ . The Fourier transform of the noise  $\tilde{n}_j(\Delta)$  is defined for the duration of the listening time window of the  $j$ th shot, an interval of roughly  $\tau_p + \tau$ . The waveforms will interact coherently with the material if the time duration of the shot is less than  $T_2$ . When the  $j$ th shot illuminates the material, its power spectrum gets burned into the absorption profile that existed before the  $j$ th shot

$$\alpha_j(\Delta) = (1 - \eta P_j(\Delta))\alpha_{j-1}(\Delta), \quad (8)$$

where  $\eta$  is a constant that depends on the material's dipole moment and spot size. In this collinear geometry, the grating is purely spectral, while for the angled beam case, some grating components are spatial-spectral and some are

purely spectral. For baseband signals modulated on  $\omega_L$ , the spectrum is a double sideband lobe that is symmetrical around  $\omega_L$ . For baseband signals modulated onto  $\omega_{RF}$  and then modulated on  $\omega_L$ , this spectral lobe is frequency shifted to  $\omega_L \pm \omega_{RF}$ . The material absorption profile can interact with one or both of these lobes.

The sinusoidal term  $\cos(\Delta\tau)$  of Eq. (7) as it appears in Eq. (8) represents a spectral grating burned into the medium that can be measured to determine the unknown delay  $\tau$ . In deriving Eq. (7), several terms were dropped, as they do not appreciably affect this result. The strong components at the optical carrier frequency are ignored since they will only burn a deep spectral hole at the optical carrier frequency. Also ignored are spectral cross terms between the return waveform and its additive noise, whose contribution to the overall noise background is small compared to that from the noise itself (i.e., assuming  $|\tilde{n}_j(\Delta)|/|\tilde{p}_j(\Delta)| > a$ ).

It is instructive to consider the simple case where there is no noise ( $|\tilde{n}_j(\Delta)| = 0$ ) and  $Ga = 1$  (i.e., identical transmit and return signals). After a single shot, the absorption profile is given by

$$\alpha_{j+1}(\Delta) \approx \alpha_j(\Delta)[1 - \gamma[1 + \cos(\Delta\tau)] - \gamma'[1 + \cos(\Delta\tau)]], \quad (9)$$

where  $\alpha_0(\Delta)$  is the absorption profile before the  $j$ th shot,  $\gamma = 2\eta\beta^2 E_0^2 \langle |\tilde{p}_j(\Delta)|^2 \rangle_\Delta$  is defined as the grating strength that represents the peak of the autocorrelation function between the transmit and return signals, and  $\gamma' = 2\eta\beta^2 E_0^2 [|\tilde{p}_j(\Delta)|^2 - \langle |\tilde{p}_j(\Delta)|^2 \rangle_\Delta]$  is a term that represents the individual strengths of the spectral components due to the autocorrelation properties of the modulating code. Thus, a Fourier transform of Eq. (9) yields processed delays, showing a strong peak at  $\tau$  due to the  $\cos(\Delta\tau)$  term proportional in strength to  $\gamma$ , and other temporal sidelobe terms at their various delays due to the  $\gamma'[1 + \cos(\Delta\tau)]$  term.

### 2.3.2. Integration

Integration has the benefit, in any radar system, of increasing the SNR of the system and allows the determination of the target velocity through Doppler processing. A straightforward extension of the preceding single shot analysis to processing

a series of radar pulses can be made with the assumption that  $T_R > T_2$ , so that the individual shots do not significantly interfere coherently with each other. After  $J$  shots, the absorption profile will then be

$$\begin{aligned} \alpha_J(\Delta) &= \alpha_0(\Delta) \prod_{j=0}^{J-1} (1 - \eta P_j(\Delta)) \\ &\approx \left( 1 - \eta \sum_{j=0}^{J-1} P_j(\Delta) \right) \alpha_0(\Delta) \end{aligned} \quad (10)$$

provided  $\eta \sum_{j=0}^{J-1} P_j(\Delta) \ll 1$  (i.e. minimal saturation). Thus, to first order

$$\begin{aligned} \alpha_J(\Delta) &\approx (1 - J\eta\beta^2 E_0^2 ((1 + a^2 G^2 + 2aG \cos(\Delta\tau)) \\ &\quad \times \langle |\tilde{p}_j(\Delta)|^2 \rangle_j + G^2 \langle |\tilde{n}_j(\Delta)|^2 \rangle_j \\ &\quad + G \langle (\tilde{n}_j^*(\Delta) \tilde{p}_j(\Delta) e^{i\Delta(jT_R)} + c.c.) \rangle_j)) \alpha_0(\Delta). \end{aligned} \quad (11)$$

In the case where the same code is used for every shot, then  $\langle |\tilde{p}_j(\Delta)|^2 \rangle_j = |\tilde{p}_0(\Delta)|^2$ , and thus integration of  $J$  exposures increases the main  $\cos(\Delta\tau)$  grating term by  $J$ . The spectral components of the undesirable temporal sidelobes associated with  $|\tilde{p}_0(\Delta)|^2$  also increase as  $J$ , while the terms with random noise increase as  $\sqrt{J}$ .

Increased gain can be achieved by using an agile coding scheme, where a different code is used for each shot, giving a combined processing and integration gain of the entire waveform series. For the processor, since each return signal is interfered with a replica of what was transmitted, matched filtering is performed for each shot. Using a different PRN code each shot, the spectral components associated with both the temporal sidelobes and noise terms in Eq. (11) are random from shot to shot and grow only as  $\sim \sqrt{J}$ . Thus, after  $J$  shots in an agile PRN code scheme, there is an enhancement in the peak to RMS sidelobe ratio of the grating by  $\sim \sqrt{J}$  over the single shot case. Agile coding also adds to the security of the radar system when the codes are generated on the fly.

The integration time also provides frequency resolution to determine the Doppler shift from a moving target according to its velocity. For range-Doppler processing, the key idea is to combine aspects of spatial multiplexing to create a bank of

parallel filtering operations. In each spatial location, Doppler processing is achieved with an offset of the optical carrier frequency of the reference waveform. Integration in each spatial location occurs at varying strengths depending on the mismatch between the optical carrier frequency and the Doppler shifted RF carrier. In other words, the Doppler shift of the target is equal to the optical carrier frequency offset of the spatial channel with the strongest integrated signal strength.

### 2.3.3. Readout

The grating readout is best accomplished by making a low bandwidth measurement of the results of high bandwidth processing, since the performance of measurement electronics is far better at lower bandwidths. The technique involves reading out spectral grating features using a low power optical pulse with linear frequency modulation (LFM) of its carrier, also called an optical frequency chirped pulse. Such a pulse has a phase continuous, linear variation in its carrier frequency at a chirp rate  $\kappa = B_{\text{ch}}/T_{\text{ch}}$  over a bandwidth  $B_{\text{ch}}$  in a duration  $T_{\text{ch}}$ . The pulse's time bandwidth product  $T_{\text{ch}}B_{\text{ch}}$  determines its spectral profile, that approaches uniformity for large  $T_{\text{ch}}B_{\text{ch}}$ . Ultimately,  $T_{\text{ch}}$  is limited by  $T_1$ , placing a lower limit on  $\kappa$  for a given  $B_{\text{ch}}$ .

Physically, the input chirped readout pulse  $E_{\text{R}}(t) = E_{\text{R}} \cos((\omega_{\text{L}} - \frac{1}{2}B_{\text{ch}})t + \frac{1}{2}\kappa t^2)$  with field amplitude  $E_{\text{R}}$ , interacts with the spectral grating, stimulating the emission of a photon echo field  $E_{\text{echo}}(t) \propto \gamma E_{\text{R}}(t - \tau)$  as a delayed replica of the readout pulse. For multiple delays there are multiple emitted output signals. Interfering the chirped photon echo with an appropriately timed reference chirp creates a temporal oscillatory signal on the intensity of the resultant optical waveform. In a collinear geometry, the transmitted chirped pulse,  $E'_{\text{R}}(t) = \sigma E_{\text{R}}(t)$ , is the input chirped reference waveform after interacting with the absorbing material, where  $\sigma$  accounts for the intensity attenuation. In an angled processing geometry, the transmitted readout pulse and echo signals are spatially distinct, providing the capability to use a reference chirped waveform that is

not affected by transmission through the absorbing material.

A photodetector (PD) performs an optical-to-electrical conversion, generating a low bandwidth analog electrical voltage  $V_{\text{out}}(t)$  that varies with time proportional to the intensity of the optical waveform  $I_{\text{out}}(t)$ . In the collinear geometry, this beat signal can be written as

$$\begin{aligned} V_{\text{out}}(t) \propto I_{\text{out}}(t) &= |E_{\text{out}}(t)|^2 = |E'_{\text{R}}(t) + E_{\text{echo}}(t - \tau)|^2 \\ &= E_{\text{R}}^2(\sigma^2 + \gamma^2 + 2\sigma\gamma \cos(\xi t + \Phi)), \end{aligned} \quad (12)$$

where the oscillation frequency is  $\xi = \kappa\tau$  and the oscillation phase is  $\Phi = (\tau/2)(-B_{\text{ch}} - \kappa\tau)$ .

By digitizing this voltage from the detector with an ADC, various digital FFT post-processing algorithms with digital windowing functions can be used to determine the PSD of the readout signal versus frequency  $f_{\text{PSD}}$ . Since the PSD represents the square of the FFT of the readout signal, the PSD peaks are proportional to  $\gamma^2$ . Scaling  $f_{\text{PSD}}$  by  $1/\kappa$  converts the frequency axis to an “extracted time delay” axis  $\tau_{\text{PSD}}$ , or

$$\tau_{\text{PSD}} = f_{\text{PSD}}/\kappa. \quad (13)$$

For a maximum resolvable time delay  $\tau_{\text{max}}$ , the required detection bandwidth is  $B_{\text{D}} = \kappa\tau_{\text{max}}$ .

Tradeoffs between higher chirp rates (desired for faster readout) and lower bandwidth limits on photodetectors and ADCs (desired for better dynamic range performance) will be necessary for any system. For example, if  $B_{\text{D}} = 10$  MHz then inexpensive 16-bit PD and ADC components can be used, where  $\tau_{\text{max}} = 2.0$   $\mu\text{s}$  and  $\kappa = 5$  MHz/ $\mu\text{s}$  corresponding to  $\kappa = 5$  MHz/ $\mu\text{s}$ . Readout of a 1.0 GHz bandwidth of the absorption profile would create a readout signal 0.2 ms in duration. For an ADC operating at 40 MSPS (x2 oversampled), the digitized output would contain 8000 points. The time required for FFT-based algorithms to calculate the PSD (e.g.,  $\sim 50$   $\mu\text{s}$  on a Xilinx Virtex-II FPGA board) adds minimally to the overall latency of the readout process.

### 2.3.4. Summary

In summary, the grating represents the power spectrum of the correlation of the transmit and

return signals. The readout signal represents a temporal map of the grating. PSD post-processing of the readout signal represents the square of the correlation of the transmit and return signals, the strength of which is proportional to the RF power of the return signal. Thus, 1 dB drop of the return signal, in RF power, corresponds to a 1 dB drop in the processed PSD peak.

The overall SNR gain of the processing and integration stages are defined in terms of the RF power of the return signal in terms as a peak-to-RMS sidelobe ratio. Thus, for processing and integration of a series of PRN sequences, the processing gain is  $\sim N$  and the integration gain is  $J$ , giving an overall gain of  $\sim N \times J$ . As an example using PRN codes, assuming  $\tau_p \sim 10 \mu\text{s}$  and a data rate of 1 Gbps (10 Gbps) and integrating 100 shots, the total gain would be  $\sim 60 \text{ dB}$  ( $\sim 70 \text{ dB}$ ). For selected code sets, where temporal sidelobes are designed to be minimal over integration of multiple shots, the enhancement can be significantly higher.

### 3. Experimental results

#### 3.1. Overview

For the experiments, a continuous wave optical carrier was stabilized to a sub-10 kHz linewidth over 10 ms. A single EOPM was used to modulate both the reference and return pulses, and a collinear beam geometry for both processing and readout. Each processing shot consisted of an  $N$ -bit BPSK waveform (i.e. radar reference signal) and a single time delayed replica (i.e. radar return signal), where shots were introduced at  $\text{PRF} = 100 \text{ kHz}$ . During any integration sequence, the delay between the waveforms in each pulse pair was fixed.

#### 3.2. Experimental setup

Fig. 2 shows the main components of the experimental setup. A cw Ti:Sapphire laser was centered at 793.380 nm and frequency stabilized to a transient spectral hole [8] in a 4 mm long Tm:YAG (0.1 at%) sample maintained at 5.0 K

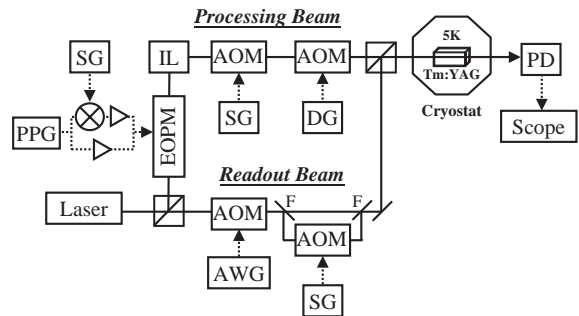


Fig. 2. Schematic of the experimental demonstration apparatus, RF mixers and amplifiers are shown symbolically (PPG = pulse pattern generator; EOPM = electro-optic phase modulator; SG = signal generator; IL = injection locking amplifier; AOM = acousto-optic modulator; DG = delay generator; AWG = arbitrary waveform generator; PD = photodetector, F = flipper mirror).

in a bath cryostat (Oxford Optistat) using a  $\sim 1 \text{ mm}^2$  spot ( $1/e^2$  diameter). The stabilized laser was split into two beams for processing and readout. The EOPM in the processing beam (Alenia Marconi, 5 GHz) was driven by a pulse pattern generator (PPG; Advantest D3186). The PPG was used to create the entire sequence of pulses (both transmit and return signal) that were programmed into the 8 MB user defined memory. Two RF paths are shown, the lower being used for baseband demonstrations and the upper for the RF carrier demonstration, with their associated amplifiers (as described below). Since a single EOPM and PPG were used, the duration of the individual coded waveforms were shorter than the processed delay. The entire processing sequence duration was 8 ms (3.2 ms) for a 1.0 GBPS (2.5 GBPS) bit rate, creating up to 800 (320) shots at the PRF of 100 kHz. After modulation, the processing beam power was  $\sim 1 \text{ mW}$ , which was then amplified to  $\sim 60 \text{ mW}$  by injection locking a higher power slave diode laser [9]. After the amplifier was an acousto-optic modulator (AOM; IntraAction ATM260C-2) driven by a signal generator (SG; HP E4432B) at +270 MHz and another AOM (Isomet 1205C-1) driven at +80 MHz (not shown) which was mixed with a delay generator (DG; SRS DG535) to easily time gate the pulse sequences.

On the readout beam path, an AOM (IntraAction ATM260C-2) was driven by an arbitrary waveform generator (AWG; Tektronix AWG610) to create a linear frequency chirped pulse around a (+270 MHz) carrier over 40 MHz at a rate of 1.1 MHz/ $\mu$ s (due to settings of the AWG). The frequency chirped pulse thus created a readout window at +80 MHz (W1) as compared to the processing signals. This chirp was timed to irradiate the crystal  $\sim 10 \mu$ s after the processing shots were completed. A high frequency AOM (Brimrose GPM1600-400) driven by a SG (HP E4432B) at 1.6 GHz was used, on a separate path accessed with flipper mirrors, to further frequency upshift the readout signal, creating a second readout window at +1680 MHz (W2) as compared to the processing pulses. For either path of the readout beam, the readout power was adjusted to  $\sim 100 \mu$ W.

Various RF signals were used for the three experiments. Fig. 3 shows spectrum analyzer traces

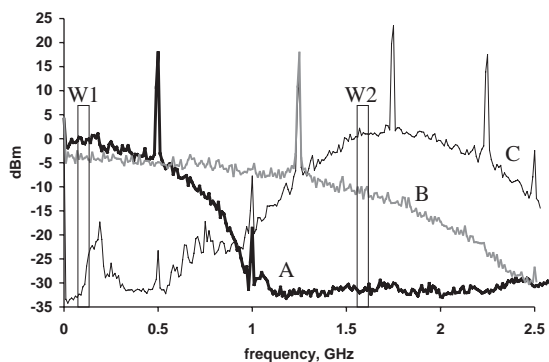


Fig. 3. RF spectrum analyzer traces of the modulation schemes used in the experimental demonstrations when repeated over several seconds. In each shot, the patterns were separated by 1.0  $\mu$ s. The shots were repeated at 100 kHz. Traces were obtained by using max-hold on the analyzer with a 1 MHz resolution bandwidth. Power levels are plotted after amplification. Trace A (bold line): 1.0 GBPS baseband modulation of 512 bit patterns, 1.0 GHz low pass filtered. Trace B (gray line): 2.5 GBPS baseband modulation of 2048 bit patterns. Trace C (thin line): 1.0 GBPS baseband modulation of 512 bit patterns, 1.0 GHz low pass filtered and mixed onto an RF carrier of 1.75 GHz. For all traces, between patterns, a square wave modulation (...010101...) was used at the respective bit rate, creating strong spectral features at half integer multiples of the bit rate, which are observed as peaks in the figure. W1 and W2 indicate regions of the spectra that were probed by a frequency scan.

of the RF signals before driving the EOPM. The three traces are listed as A, B and C, which each were generated using an RF spectrum analyzer (Rohde & Schwarz FSEM30) on max-hold mode with a 1 MHz resolution bandwidth, where signals were repeated for several seconds. These typical processing sequences employed dynamic coding for each shot, where each processing shot contained a unique, zero-mean BPSK waveform and its time delayed replica. In case A (bold line), the PPG bit rate was 1.0 GBPS, the patterns were 512 bits long (512 ns) and a 1 GHz low pass RF filter was used (not shown in Fig. 2) and the signals were amplified (Veritech VM2.5EMD-422) to 5.0 V and fed to the EOPM (lower path in Fig. 2). The main lobe of the modulation to 1 GHz is due to the random pattern set being repeated over the repeating 8 ms window. Strong frequency component spikes at ( $\frac{1}{2}R_B, R_B, \frac{3}{2}R_B, \dots$ ) can be observed on the traces, which were created by square wave (...101010...) modulation at the bit rate  $R_B$  between patterns. These signals are used as frequency markers that become spectral holes burned into the spectrum. While this modulation is shown, it could be turned on and off in the experiments with no appreciable change to the readout signals that are presented here. The case in trace A was used for the majority of the experimental results below. Trace B shows the case when the PPG bit rate was 2.5 GBPS and patterns of 2048 bits long (819.2 ns) were used, along with the same amplifier as in trace A but without filtering (lower path in Fig. 2). The main lobe is observed over 2.5 GHz with a strong frequency spike at 1.25 GHz. Trace C shows the case for IF modulation, where the same signal that generated trace A was then mixed onto a 1.75 GHz carrier using an RF mixer (Teletech MC36A) that was driven by a signal generator (Agilent E4432B) at 17 dBm and then amplified by a broadband high power RF amplifier (HP/Agilent 83020A) before being fed to the EOPM (upper path in Fig. 2). Fig. 3 also shows the location and spectral width of the readout windows W1 and W2 (described previously) in relation to the RF signals.

A cube combined the processing and readout beams, which were focused to a  $\sim 50 \mu$ m spot in the sample. After the sample the beams were

incident on a photodetector (PD; New Focus 1801) that was AC coupled (25 kHz–125 MHz). A digital oscilloscope (Tektronix TDS3054) was used to digitize the traces at 12.5 MSPS over a fixed 40  $\mu\text{s}$  window (500 points). While better digitizers will be used for future work, in this case their dynamic range was not exceeded.

### 3.3. Results

A typical example of the readout signal intensity variation is shown in Fig. 4(a) for the processing configuration of Fig. 3, case A, with a delay of 1.0  $\mu\text{s}$  between processing pulses, after 800 inte-

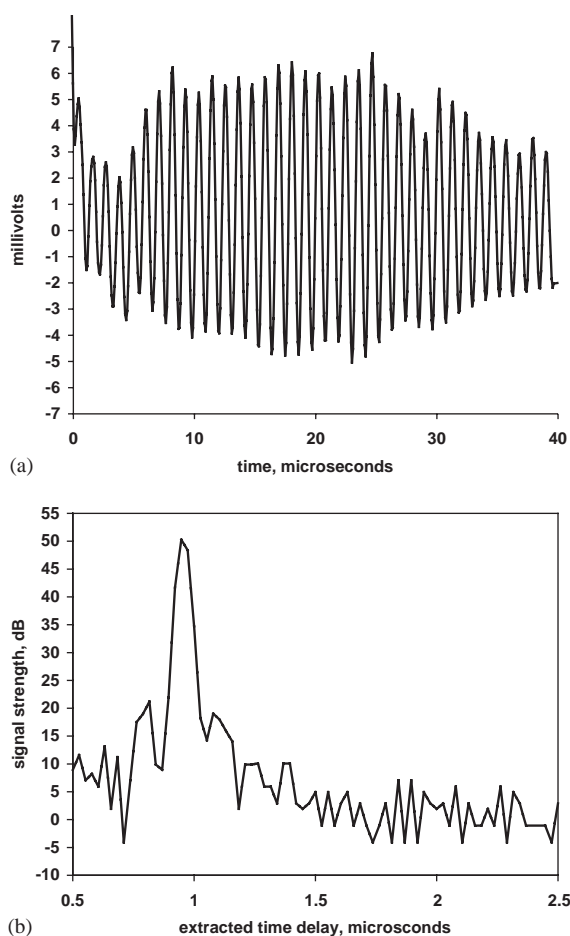


Fig. 4. (a) Example time domain readout signal and (b) resultant power spectral density signal showing signal strength versus extracted time delay. The peak at 1.0  $\mu\text{s}$  matches the delay between patterns.

grated shots. The figure shows approximately 36 cycles in the 40  $\mu\text{s}$  readout window, consistent with  $\kappa = 1.1 \text{ MHz}/\mu\text{s}$ . Fig. 4(b) shows the calculated PSD of the signal in Fig. 4(a), where a Hanning window was applied, and the x-axis was converted to extracted time delays using Eq. (13). The peak width ( $\sim 25 \text{ ns}$  FWHM) corresponds to the limited readout bandwidth. The signal strengths are plotted in units of decibels (dB), and shown in relation to the noise floor (set to 0 dB). The main delay at 1.0  $\mu\text{s}$  has strength of 50 dB with a maximal sidelobe level on the order of 20 dB, showing a spur free dynamic range of 30 dB.

The next series of results were taken for the 1.0 GBPS baseband modulation case (W1 on trace A), with the largest observed signal strengths under these limited (collinear geometry, 40 MHz readout window) conditions. Fig. 5 shows the results of processed time delays that were varied over 0.6–1.0  $\mu\text{s}$ , extracted from the PSD of transmitted readout signals, after 200 shots. The processing beam power was 2.5 mW in this case. The peaks are shown to match well with the processed time delay, and calculations of several captures at the same delay showed  $< 3 \text{ ns}$  jitter (readout bandwidth limited). The decrease of the peak signal with increasing time delays is due to the material coherence time. Higher temporal resolution and dynamic range is expected at higher readout bandwidths.

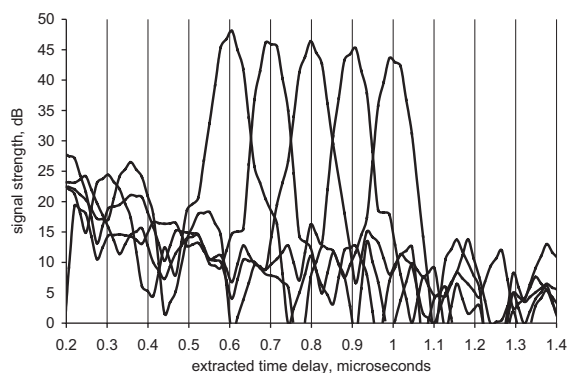


Fig. 5. Time delay variation from 0.6 to 1.0  $\mu\text{s}$  for processing signals of trace A with W1 scan, showing  $> 40 \text{ dB}$  dynamic range for these conditions. The scan was taken after 200 shots at 100 kHz, where each shot consisted of a unique dynamic 512 bit pattern and its replica at 1 GBPS BPSK modulation.

Fig. 6 shows the behavior of the signal strength enhancement achieved by integration of multiple coherent processing results. The peak strength of

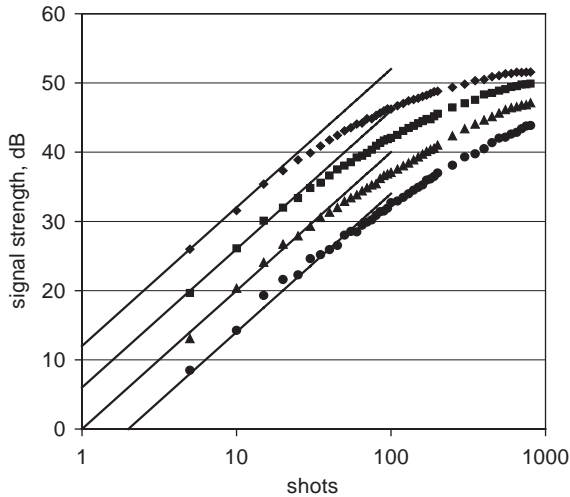


Fig. 6. Integration dynamics plotted as peak strength versus  $J$  processing shots for various processing beam powers. The processing power was 2.5 mW for the diamonds and decreased by factors of 2 in optical power to 0.31 mW for the circles. The data compared with ideal integration behavior  $P^2 J^2$  (the solid lines are offset from each other by 6 dB), showing saturation after a number of shots that depends on  $P$ .

the readout signal peak, in dB, is plotted versus the number of processing shots on a log scale, up to 800 shots, with a fixed 1  $\mu$ s delay, for four different processing beam powers  $P$  of 2.5 mW (top trace), 1.25, 0.625 and 0.3125 mW. Each data set individually shows that the processed signal strength initially grows ideally as  $J^2$  (solid lines), as expected, but then exhibits power dependent roll-off due to saturation before reaching a steady state. For 0.3125 mW, the saturation point is roughly 85 shots, while for 2.5 mW it is roughly 15 shots. The various data sets show that the signal strength varies as the optical power squared in this configuration (each line offset by 6 dB), due to the effect of increasing the optical power of both the reference and return signals by 3 dB.

Fig. 7 shows the effects of dynamic coding for each shot as compared to using a single code repetitively shot to shot. The processing beam power was 2.5 mW. (a) Plots the peak and RMS left sidelobe (LSLRms) level as calculated over a time window from 0.5 to 0.9  $\mu$ s, in dB, versus shots (log scale) to observe their evolution during integration. Fig. 7(b) shows the corresponding extracted delay profile after 800 shots. For both agile processing and a single code, the peak strengths grow identically as  $J^2$  and then rolls off as in the previous figure. For the single repeated

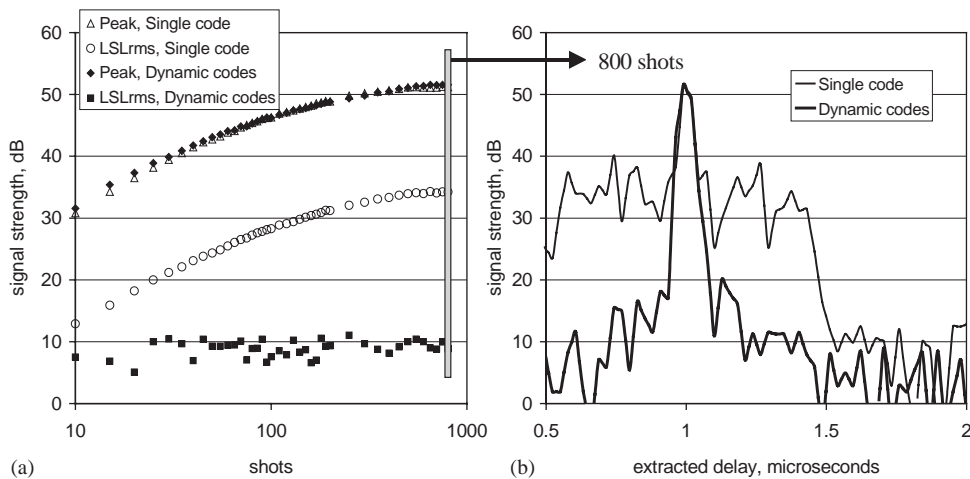


Fig. 7. The effect of agile processing with dynamic patterns is shown. In (a), the 'Peak' and the calculated RMS left sidelobe 'LSLRms' values are plotted for both agile processing of dynamic patterns and integration with a fixed pattern for each shot. In (b), the range profile after 800 shots for single and dynamic codes is shown. The system noise floor is defined as 0 dB. The ratio of the peak to 'LSLRms' is greater than 40 dB.

code case, LSLrms grows with the peak, while for dynamic coding these change shot to shot. For the particular single code used, the calculated peak to LSLrms was  $\sim 18$  dB, which is maintained between the peak and LSLrms throughout the integration series. For the dynamic coding case, the LSLrms level is shown to fluctuate around 10 dB. While this level is expected to grow with  $\sim J$ , here the LSLrms level for dynamic coding is lower than the artificially high noise floor at  $\sim 10$  dB. After 800 shots, a peak to LSLrms level of 42 dB is observed, giving an enhancement of  $\sim 25$  dB in the dynamic range after 800 shots due to the spread spectrum nature of the PRN code set.

Fig. 8 shows typical single capture results for the cases dealing with extended processing capabilities.

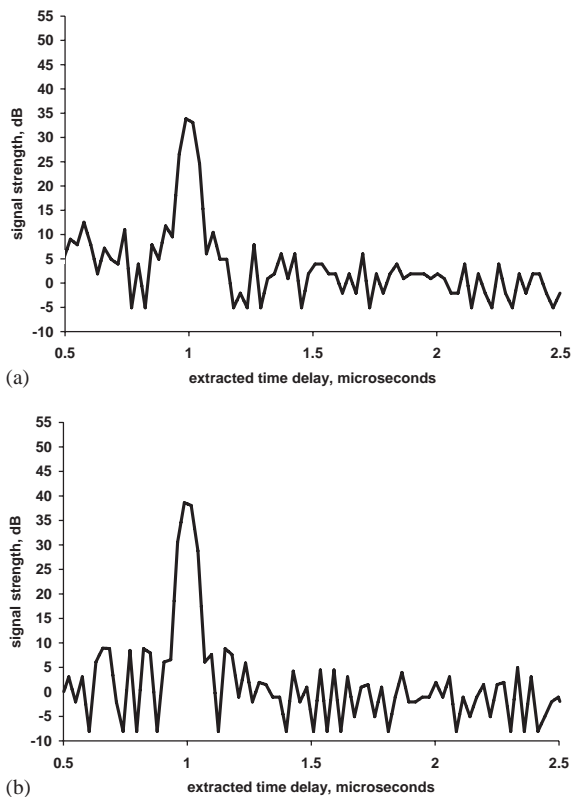


Fig. 8. Typical post-processed range results for 2.5 GBPS baseband and 1.0 GBPS IF processing. (a) Baseband processing of 2.5 GBPS signals, corresponding to trace B of Fig. 3 with W1 scan. (b) RF carrier processing of 1.0 GBPS signals modulated on 1.75 GHz, corresponding to trace C of Fig. 3 with W2 scan.

Fig. 8(a) shows a post-processed result for the 2.5 GBPS baseband modulation case, corresponding to trace B in Fig. 3 when using W1 after 320 shots. It should be noted that W2 on trace B was also used, and showed similar but weaker main peak strength (by  $\sim 10$  dB). Fig. 8(b) shows a similar result for the case of 1.0 GBPS modulation on an RF carrier, corresponding to trace C in Fig. 3 when using W2 after 800 shots. The similarity of the graphs is the main result of these proof-of-concept experimental efforts, where gratings were observed with varying strengths. Beyond the results shown, other readout windows were accessed by tuning the signal generators of both the +270 MHz AOM in the processing beam and the +1600 MHz AOM in the readout beam, thereby moving W1 and W2 to observe other parts of the grating, which gave similar results to those shown here.

#### 4. Summary

In summary, multi-GHz coherent signal processing and integration of up to 800 dynamically changing shots was demonstrated under three different experimental conditions. The demonstrations used a Tm doped YAG crystal held at 5.0 K, a  $\sim 1$  mW beam from a frequency stabilized continuous wave laser, commercially available telecom components, and a low-power chirped pulse probe. Time delays up to  $1.0 \mu\text{s}$  were processed and extracted with over 40 dB of dynamic range under limited readout capabilities. We believe that the techniques introduced here represent substantial progress towards a practical, high performance analog coherent integrating temporal signal processor with the necessary bandwidth, frequency resolution, integration time and dynamic range for modern radar systems.

#### Acknowledgements

The authors gratefully acknowledge the support from NASA Ames Research Center under grant NAG2-1323, from the Montana Board of Research and Commercialization technology under

grant Z3143, and also wish to thank Kelvin Wagner, University of Colorado, Boulder, for conceptual contributions and useful discussions.

## References

- [1] Z. Cole, T. Böttger, R. Krishna Mohan, R. Reibel, W.R. Babbitt, R.L. Cone, K.D. Merkel, *Appl. Phys. Lett.* 81 (2002) 3525.
- [2] V. Lavielle, I. Lorger, J.-L. Le Gout, S. Tonda, D. Dolfi, *Opt. Lett.* 28 (2003) 384 and references therein.
- [3] I.I. Popov, V.V. Samartsev, *Atmos. Oceanic Opt.* 14 (2001) 411.
- [4] R. Reibel, Z. Barber, M. Tian, W.R. Babbitt, *J. Lumin.* 98 (2002) 355 and references therein.
- [5] X. Wang, M. Afzelius, N. Ohlsson, U. Gustafsson, S. Kröll, *Opt. Lett.* 25 (2000) 945.
- [6] J.C. Toomay, *Radar Principles for the Non-Specialist*, 2nd Edition, SciTech, 1998.
- [7] J.Z. Peebles, *Radar Principles*, Wiley, New York, 1998.
- [8] M. Strickland, P.B. Sellin, Y. Sun, J.L. Carlsten, R.L. Cone, *Phys. Rev. B* 62 (2000) 1473.
- [9] R.R. Reibel, Z.W. Barber, M. Tian, W.R. Babbitt, Z. Cole, K.D. Merkel, *J. Opt. Soc. Am. B* 19 (2002) 2315.